Final report

Ex vivo cultivation of bipolar epithelial/endothelial cell layers as a first step towards an organ like alveolar barrier

Leibniz-Institute: DWI - Leibniz-Institut für Interaktive Materialien Aachen

Reference number: SAW-2015-DWI-2471

Project period: March 2015 – Feb 2018

Contact partner:

Prof. Dr. Martin Möller, DWI - Leibniz-Institut für Interaktive Materialien Aachen

Stand: 04. Dezember 2015

Executive Summary

Organ level barriers are typically formed by bipolar layers of different kinds of cells separated by a basal lamina membrane. The cells on both side of the basement membrane, control each other regarding their proliferation, morphogenesis, and function by chemokines and mechanical cues. For development of such organ level barriers up to recently synthetic poly(carbonate) or poly(dimethylsiloxan) membranes were employed. These membranes are microporous to allow exchange of chemical signals. However, these synthetic membranes still remains far from *in vivo* basement membrane in terms of barrier thickness, cellular composition and mechanical stimulation. To overcome this, in this project we focused on ultrathin nanofiber membranes prepared by electrospinning techniques which is equipped with ligands for cell adhesion e.g. laminin and fibronectin derived peptides to promote selective cell adhesion. The thickness of these nanofiber membranes resembles the structure of the basement membrane. Moreover the interconnected pores of the membrane provide better cell-cell contact and exchange of paracrine signals. The nanofiber membrane is prepared with tailored biodegradability i.e., constituted from bioresorbable components, so that the synthetic membrane could be replaced in due time by native components secreted by the cells grown on the nanofiber membrane. Alveolar barrier was mimicked by establishing first a bipolar followed by a tripolar culture. For bipolar culture monolayer of primary lung endothelial and epithelial cells were seeded onto the different sides of the nanofiber membrane. This e*x vivo* bipolar alveolar barrier was studied with regards to the barrier properties, formation of a natural basal lamina membrane and the viability of the cells. Furthermore to gain first insights into possible lung inflammatory reactions in *in vitro,* this co-culture model was expanded by a human leukaemia monocyte cell line (THP-1). This triple-culture system was established on a basement membrane mimic, maintaining the barrier properties of the bipolar co-culture. To mimic the hemodynamic of the lung microvasculature a multi-functional microfluidic device was fabricated using polyjet 3D printing. The device constitutes two flow chambers, one for the blood side and one for the bipolar alveolar barrier. The cytotoxicity of the chamber was tested and as a proof of principle anticoagulant hydrogels coatings were implemented to make the device more compatible for blood flow. For functioning of the device under physiological cell-culturing conditions the inner design of the cell-culturing device especially the round shaped diameter of the bioresorbable fleece/membrane was adapted to implement growth under a fluctuating tidal strain of the alveolar blood-air barrier of maximal 4 % at 8 mbar transmembrane/pulmonary pressures. As a distinctive feature of the microfluidic device, pressure can be applied to deform/expand the membrane for mimicking the expansion and relaxation of the alveolar barrier in the lung. The results obtained form the proposed project intended to (i) generate new insights in the *ex vivo* reconstitution of alveolar barriers, (ii) to establish a model for mechanistic *in vitro* studies on the action of drugs, lung surfactants and environmental pollutants, and (iii) open the route for novel disease models. Further the project lays the ground for the *ex vivo* reconstruction and studies of other natural barriers e.g. endothelial based boundaries in multicellular organs.

1. State of the Art

Organs represent complex structures consisting of different cell types with discrete yet interdependent functions. *In vitro* construction of living tissue or organ models from cell cultures suffers from the fact that we can barely provide and control the diverse cues needed to emulate the *in vivo* interaction of cells that enable their viability and function. Only during the last decade have tissue engineering concepts been advanced from using basic structural scaffolds towards novel strategies that focus on paracrine effects, i.e. directed constitution of functional cell-cell contacts and interconnectivities in three dimensions. For this purpose researchers have employed decellularized tissue as a quasi-natural scaffold[1] or developed synthetic scaffolds that have been equipped with specific cell-adhesive sites and linkages that can be reconstructed or remodeled by the cells.[2-4] An alternative approach focusses on microtissues comprising a limited number of cells assembled to a functional network which will then provide a basis for hierarchical tissue engineering. A prominent example is given by stacked cell-sheets cultivated as confluent 2D-layers with their own functional extracellular matrix (ECM).[5] Controlled and directed 3D-assembly of single cells was reported by Bertozzi and Gartner who functionalized cells with short oligonucleotides to impart specific cell-cell adhesive sites.[6] More recently a cell accumulation technique was reported where isolated single cells were preconditioned by ECM-proteins to promote their spontaneous assembly in three dimensions.[7] These concepts have led to entirely new and extremely promising hetero-cell tissue models in which contacts between different cell types can direct the differentiation from an unstructured cell assembly to an organized and functional micro-tissue. A particular example of a functional hetero cell-contact is found in the endothelial/epithelial barriers that confine organ compartments such as alveoli in the lung (blood-air-barrier). Hetero-cellular organ models are promising alternative to existing cell and animal models with poor predictive power due to great difference in anatomy. An alveolar barrier at the bronchial tree in lung constitutes of bipolar layers of epithelial and endothelial cells separated by a semipermeable thin basement membrane (BM) of extracellular matrices (ECM) and functions as blood-air interface for gas exchange, fluid homeostasis, cell-cell crosstalk, and defense system.[8, 9] Modeling normal lung functions and adverse events including pulmonary edema, rhinosinusitis, and chronic obstructive lung diseases, contribute to advanced drug discovery system and safety test.[10] To this end, *in vivo*-like hetero-cellular bipolar culture models[11-15] have attracted increasing attention than cell monolayers that lacks dynamic cell-cell crosstalk and synergistic response.[16, 17] Ingber and others designed a bipolar lung model in microfluidic system with mechanical stimulation.[14] However, these methods have not recapitulated organ-level barrier functions so far because these membranes used as a BM were not bioresorbable and there are structural differences from natural one comprising ultrathin fibrous sheet with interconnected pores. Moreover, these membranes lack functionalization with

specific ligands for alveolar cells, which prevent long term adhesion of sensitive primary cells.

In natural BM, specific ECM proteins such as laminin (LM), collagen type IV, and proteoglycan form thin mesh-like structures (0.1 to 1 µm) crosslinked with randomly oriented nanoscale fibrils.[18] Interconnected nanopores allow for selective transfer of cells and signaling molecules and ECMs regulate cellular functions, which contributes to tissue morphogenesis, homeostasis, and disease pathogenesis. Although natural BM is extensively studied,[19-21] the development of BM mimics is still challenging, which arises due to the difficulties in recapitulating nanostructures, multi-functionality of BM, and robustness. Therefore, to achieve better cellular function there is a critical need to develop an advanced synthetic BM mimic with micro/nanoscale topography, mechanical robustness, and biocompatibility.

In this project we focused above the current state of art (i) by replacement of the thick artificial membrane used in the *in vitro* devices described above by an ultrathin nanofiber membrane which mimics the basal membrane on which alveolar-capillary barrier model was established. The alveolar barrier was reconstituted by seeding endothelial and epithelial cells onto the different sides of the nanofiber membrane. We studied the e*x vivo* cultivation of bipolar epithelial/endothelial cell layers with regard to the formation of a natural basal lamina membrane and the viability of the cells. The bipolar culture was subjected to air-liquid interface, and production of surfactant on the epithelial side was estimated. We compared the barrier structure and permeability to conventional porous film and evaluated biodegradability of mesh. To gain first insights into possible lung inflammatory reactions in *in vitro,* this co-culture model was further expanded by a human leukaemia monocyte cell line (THP-1) (ii) to transfer the principles to a microfluidic organ-like membrane module where the endothelial layer is in direct contact with the blood pumped through the device, we developed a microfluidic device which mimics the hemodynamic of the lung microvasculature. The results are discussed further in detail below with respect to different work packages.

2. Work Packages

For the successful accomplishment of the project the work flow was divided into five work packages:

WP I: Synthesis of a bioresorbable basal membrane mimic (DWI-Aachen). **WP II:** Designing of the microfluidic cell culturing and oxygenator device (DWI-Aachen). **WP III:** Site-specific seeding of the barrier membrane by alveolar epithelial and micro- vascular endothelial cells (UMC-Mainz). **WP IV:** Cyto- and hemocompatibility evaluation and modification of the oxygenator device (IPF-Dresden). **WP V:** Proof of principle, establishment of the Air-Blood interface (UMC Mainz)

3. Result and Discussion

3.1 Preparation of nanofiber mesh and evaluation of structures

To develop natural basement membrane mimics with ultrathin meshwork structures in the working group of Prof. Martin Möller, fiber meshes were fabricated by electrospinning technique. Electrospinning technique is a manufacturing technology for ultrafine continuous fibers ranging from ca. 10 nm to over 10 µm in diameter.[22] When high voltage is applied to a polymer solution at a spinneret and electrostatic repulsion exceeds surface tension of the solution, a Taylor cone produces polymer jets, resulting in the formation of ultrafine fibers on a target through solvent evaporation. The properties of the fibers, including material composition and structure (diameter, morphology, and stiffness) can be tuned, and this facile, versatile technique has received great interest for material engineering and biomedical applications.[22-25] Due to this dynamic fabrication process, complex interplays of parameters determine the morphological and chemical features of the fibers. We previously reported fabrication of electrospun polyester micrometer-sized fibers with NCO-sPEG as a functional additive for controlled surface chemistry.[26, 27]

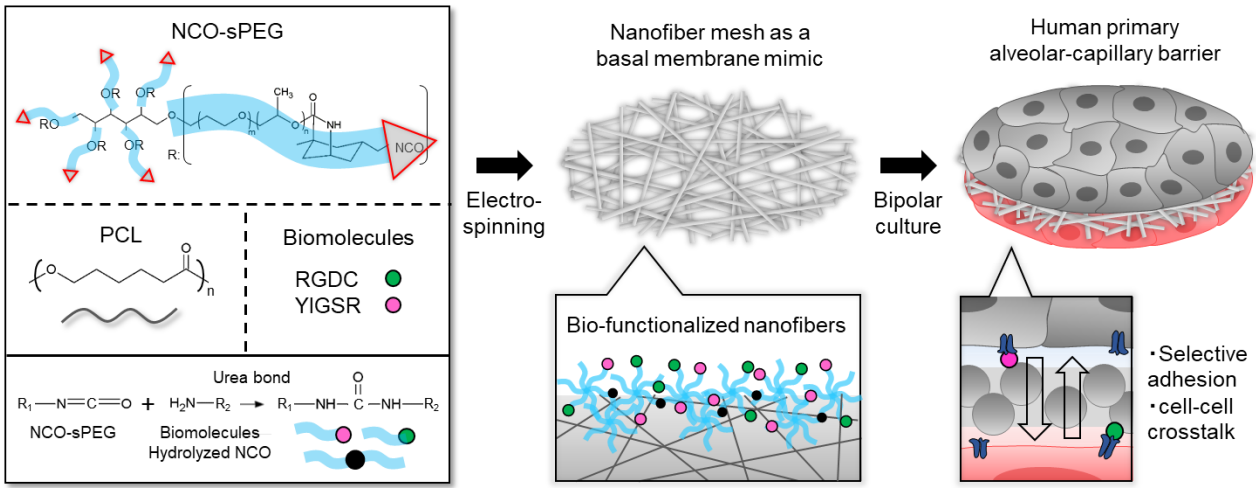

Scheme 1: *Schematic illustration of the fabrication process of the alveolar barrier model. (a) Illustrated in the scheme are the chemical structures of polymers used in this study. NCO-sPEG with hydrophilic chains and NCO end groups for conjugation of biomolecules and bioresorbable PCL. (b) Nanofiber mesh as a BM mimic was formed by electrospun nanofibers of PCL-sPEG functionalized with biomolecules. (c) Human primary epithelial and endothelial cells were bipolar-cultured on nanofiber mesh to reconstruct an alveolar barrier models capable of cell-cell crosstalk.*

Functional star-shaped PEG has the advantage of its hydrophilicity for the prevention of unspecific protein adsorption and provides mechanical strength of fibers by intermolecular crosslinking as compared to linear PEG.[28, 29] Moreover, we found that these fibers possessed core (PCL) and shell (sPEG) like structures by electrostatically driven surface segregation,[22] leading to bio-functional fiber surfaces with sPEG and peptides.[30] We employed this functional fiber to develop thin BM-like meshes of nanofibers modified with bioactive molecules by changing the parameters of the preparation. PCL, which is a cytocompatible, slowly-degrading polyester,[31] and sPEG (4:1 in weight ratio) were dissolved in several sol-

vents with different solubility, conductivity, and boiling point. First, 6 wt% PCL and NCO-sPEG (20 wt% to PCL) were dissolved in 1,1,1,3,3,3-hexafluoroisopropanol (HFIP) and trifluoroacetic acid solution was then added to increase the conductivity.

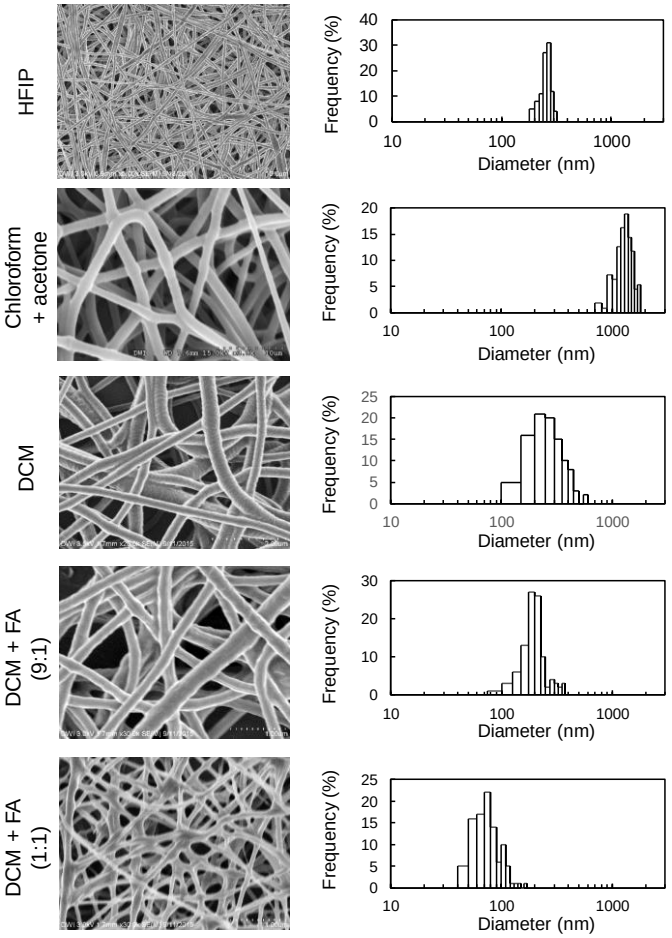

Figure 1. *Fabrication of electrospun nanofibers. SEM images and diameter distribution of electrospun fibers with different solvents (HFIP, the mixture of chloroform and acetone, DCM, and the mixture of DCM and FA). The diameter was measured from SEM images (three different samples, 100 fibers were measured in total).*

When the polymer solution was pumped at the rate of 0.5 mL/h and 20 kV of a positive high voltage potential was applied to the collector, uniform polymeric fibers were deposited on the aluminum foil. A scanning electron microscopy (SEM) image shows PCL-sPEG nanofibers with a narrow distribution in width around an average diameter of 260 nm (**Figure 1 top**). Alternate electrospun conditions with different solvents (chloroform and acetone, DCM, and DCM with FA (9:1 or 1:1)) yielded fibers that were less uniform regarding their diameter, shape, and the pore sizes of the mesh (**Figure 1**). For the BM-mimicking application envisioned here, the fiber diameter should be of the nanometer scale with only a few micrometer-thick filaments and pore sizes smaller than 5 µm.

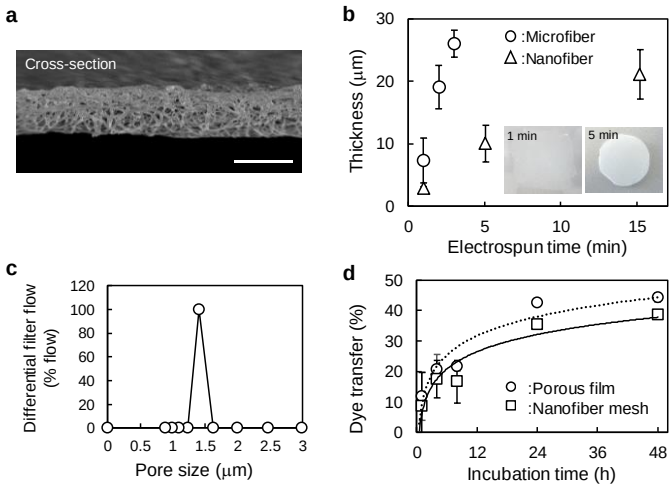

Figure 2. *Characterization of nanofiber meshes. (a) Cross-sectional SEM images of PCL-sPEG nanofibers. (b) The relationship between electrospinning time and thickness of the mesh (n=5). The insets depict the nanofiber mesh after 1 and 5 minutes of electrospinning. (c) Pore size distribution of PCL-sPEG nanofiber mesh with 10 µm of thickness measured by a capillary flow porometry. (d) Dye transfer of Rhodamine-labelled BSA across porous films with 3 µm of pores and nanofiber mesh (n=3). Scale bar, 20 µm.*

The cross-sectional SEM image in **Figure 2a** demonstrates interconnected network spaces in the PCL-sPEG mesh. The mesh thickness was controlled by the deposition time of elec-

trospun fibers (**Figure 2b**). We prepared the thinnest mesh after 1 minute of electrospinning with a thickness of 2 µm. The PCL-sPEG nanofiber mesh with thickness of 10 µm possessed an average pore size of 1.5 µm (**Figure 2c**). Such a nanofiber mesh had a similar permeability as the membrane with 3 µm pores of the original transwell insert (**Figure 2d**). In both cases, the pores were sufficiently small to separate cells and to prevent their migration through the mesh. In the case of the nanofiber mesh, however, the porosity was determined to be 71% compared to 14% of the original transwell membrane (Porosity P = (1 - d_m/d_p) x 100 (d_m: density of mesh, d_p: density of PCL 1.145 g/cm^3).[24] The high-porosity improves the transport of small signal molecules for hetero-cellular crosstalks. For the benefit of easy handling, nanofiber meshes of 10 µm thickness were used in the following experiments.

3.2 Mechanical property of mesh

An important aspect for the design of synthetic basement membrane for an alveolar barrier is their mechanical strength against cyclic strain. During breathing the barrier is mechanically stretched by 5% to 15%.[32] **Figure 3** demonstrates uniaxial stress-strain measurements for a PCL-sPEG nanofiber mesh of 10 µm thickness. The Young's modulus achieved a value of 5.2 MPa referring to the cross section of the mesh (**Figure 3a**). We mimicked the repetitive tissue stretching during breathing by 30 strain-relaxation cycles of 15% at 0.25 Hz and observed little to zero hysteresis or creep (**Figure 3b**). Even thinner nanofiber mesh with 2 µm of thickness showed good stability against cyclic strain (**Figure 3c**). PCL is a semicrystalline polymer with rubbery properties and intermolecular crosslinking between sPEG with amine and NCO group enhanced the mechanical stability.

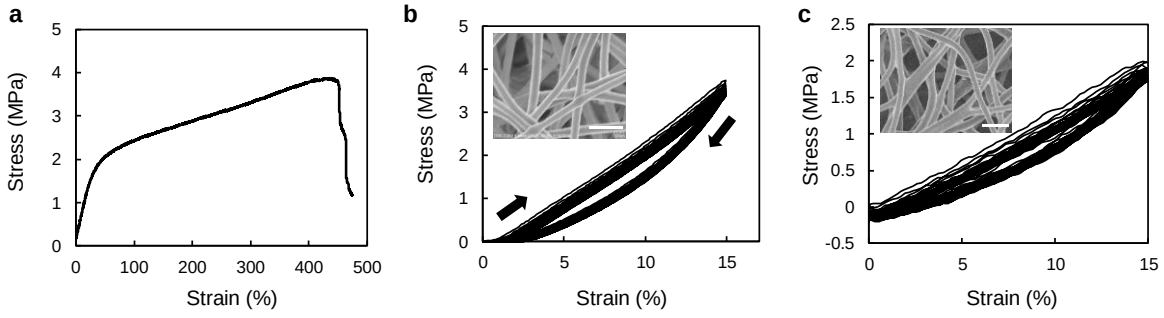

Figure 3. *Mechanical property of nanofiber mesh. (a) Stress-strain curve of 10 µm of nanofiber mesh in thickness by a tensile tester. The cyclic strain test (15% x 30 times) of (b) 10µm and (c) 2 µm of nanofiber mesh. The insets show SEM images of the nanofiber mesh after the test. Scale bars, 1 µm.*

3.3 Surface chemistry of nanofiber

Fundamental activities of epithelial and endothelial cells are regulated through the interaction with specific ligands in ECMs. To provide this ability in our engineered nanofiber meshes, we functionalized them with various peptides by addition of amine groups to NCO-groups of the star-PEG molecules. Peptides with free amine groups (lysine or N-terminus) were added to the solution of PCL and NCO-sPEG in HFIP and incubated for 1 hour before the solutions were electrospun. Kinetically favored reaction of the isocyanate groups with the amine ena-

bled this one step procedure. The confocal scanning laser micrograph (CLSM) shown in **Figure 4a** demonstrates the successful modification of the fiber surface with the example of fluoresceinamine as a model reaction for the peptide modification. The fluoresceinamine modification was quantified by measuring the fluorescence intensity in the supernatant to obtain the amount of unmodified fluoresceinamine. We found that a range of 0.02 to 29 µg of fluoresceinamine per 1 g of nanofiber mesh was modified. Covalent binding of fluoresceinamine can be increased by a larger ratio of amine to NCO-sPEG. The modification proceeded at high efficiency (66-80%) (**Figure 4b**). Because of the surface segregation of the NCO-sPEG molecules,[26] the peptides introduced by this procedure will be presented at the surface of the nanofibers. Here, surface segregation of the NCO-sPEG molecules was confirmed by the observation that the meshes readily wetted by water and substantially suppressed unspecific protein adsorption (**Figure 4c**). This non-fouling property is important to achieve specificity in the interaction with membrane proteins of the cells and to avoid unwanted cell reactions to adsorbed and eventually denatured proteins present in the medium.[33]

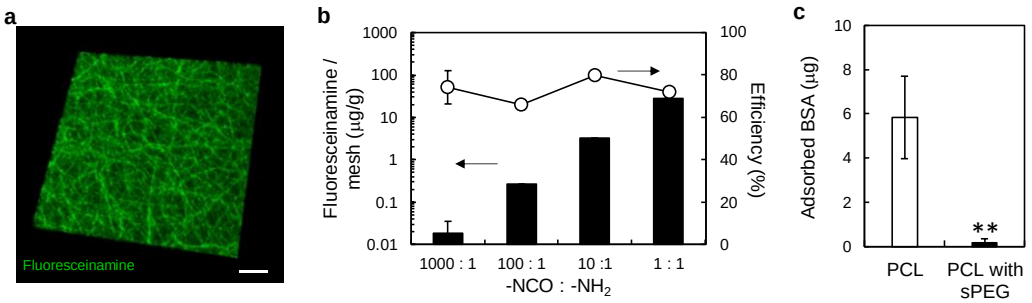

Figure 4. *Surface chemistry of the nanofiber mesh. (a) 3D-reconstructed CLSM image of nanofibers labeled with fluoresceinamine. (b) The measurement of the amount of fluoresceinamine modification of PCL-sPEG nanofibers and reaction efficiency (n=3). The stoichiometric ratio of fluorescein amine to NCO-sPEG was varied from 1000:1 to 1:1. The fluorescence intensity of the supernatant washing solution containing unmodified fluoresceinamine was measured. (c) BSA adsorption to PCL and PCL-sPEG mesh (n=3). **P<0.01 when compared with PCL. Scale bars, 20 µm.*

3.4 Effect of biofunctionalization on cell adhesion

For ligand affected cell adhesion, we decorated the nanofiber meshes with cell adhesive peptides. In a first series of experiments this was studied with cells from a human lung carcinoma cell line (NCI H441) and human umbilical vein endothelial cell (HUVEC). The purpose was to find optimum cultivation conditions that could be transferred to the more sensitive cultivation of primary human pulmonary alveolar epithelial cells (HPAEC) and primary human pulmonary microvascular endothelial cell (HPMEC). Peptides were mixed with PCL and NCO-sPEG solution at a molar sPEG-to-peptide ratio of 5:1 and incubated for 1 hour before electrospinning. After the electrospinning and sterilization by UV exposure, human cells were seeded onto the nanofiber mesh and cultured for 2 days. The SEM images in **Figure 5 a** and **b** show NCI H441 cells that adhered on a nanofiber mesh that was equipped with RGD peptides, a conserved fibronectin-fragment responsible for integrin-mediated ad-

hesion. The picture resembles closely the situation found for cells that adhere *in vivo* to natural ECM fibers. The adhesion and proliferation of HUVEC increased, when the surface concentration of the RGD peptide was increased. We consider that this is a phenomenon affected by the surface bound peptides. The cyclic peptide RGDfC (cyclic RGD, where f denotes an F residue having the d configuration) demonstrated a similar strong adherence, while a scrambled form of RGD peptide (RGES) did not promote cell adherence.

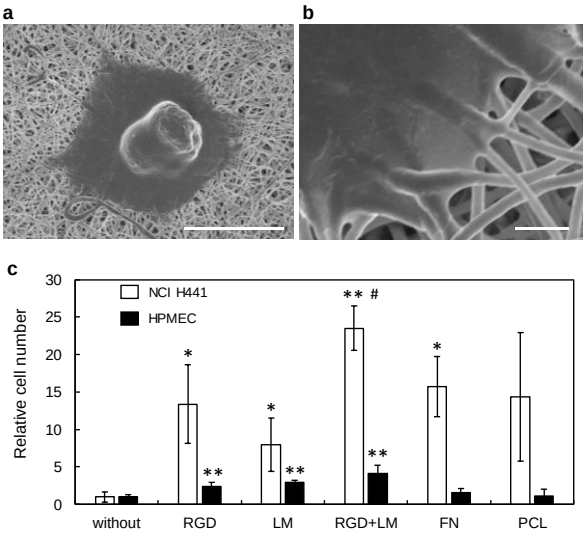

Figure 5. *Optimization of peptide mediated cell adherence. (a) SEM image of NCI H441 cells cultured for 2 days on a PCL-sPEG nanofiber mesh modified with RGD peptide. (b) Magnified SEM image of NCI H441 cells. (c) Cell adhesion tests of NCI H441 and HPMEC to nanofiber mesh modified with RGD, LM, RGD+LM (1:1 at molar ratio), and FN (n=4) after 2 days of culture. The PCL-sPEG nanofiber meshes without peptide and PCL nanofiber mesh were used as controls. *P<0.05, **P<0.01 when compared with and without (Student t-test). #P<0.05 when compared with LM (Tukey's multiple comparison test). Scale bars, 1 µm (a) and 20 µm for (b).*

3.5 Comparison of different cell ligands

We compared different cell ligands for cellular adhesion, including RGD peptide, YIGSR peptide from LM β1 chain (LM peptide), their combination, and fibronectin for cellular adhesion. PCL-sPEG and a pure PCL mesh without peptides were used as a control. While NCI H441 and HPMEC cell adherence was suppressed on the PCL-sPEG nanofiber mesh without peptide, it was significantly increased when the ligands were introduced in the fiber surface **(Figure 5c**). The combination of RGD and LM peptides (at a 1:1 molar ratio) yielded the most pronounced adherence effect for NCI H441 cells. This is partly explained by the complementary action of the RGD and the LM ligands that interact specifically interact with different integrin receptors such as integrin α5β1, integrin αvβ3, and receptor against laminin. In addition, there may be synergetic signaling with multiple receptors.[34]

3.6 Structural observation of bipolar barrier

Based on the results above, PCL-sPEG nanofiber mesh with RGD and LM peptides were employed for bipolar cultivation. The nanofiber meshes were cut into discs of 1 cm in diameter and fixed to transwell insert, and then the cells were seeded on the top and bottom separately. Confocal microscopy images displayed formation of a confluent bipolar barrier of NCI H441 and HUVEC by seeding cells at high density (1 x 10^5 cells/0.33 cm^2). Transmission electron micrographs (TEM) confirmed the formation of a bipolar interface between the two cell types comprising confluent layers of NCI H441 with cuboidal morphology and HPMEC

with flattened morphology and adherence junctions. Within the NCI H441 layer, **Figure 6b** depicts microvilli (Mv), tight cell-cell junctions (TJ) and adherent junction (AJ) complexes accompanied by a desmosome at the apical membrane. The confocal microscopy image in Figure 7c confirms the formation of a confluent barrier structure and demonstrated furthermore the formation of lamellar bodies (LB) indicating the production of lung surfactant. LBs were marked by staining with quinacrine.[14] The surfactant production showed a 3.7-fold increase after differentiation induced by air/liquid interface culture (**Figure 6d**).

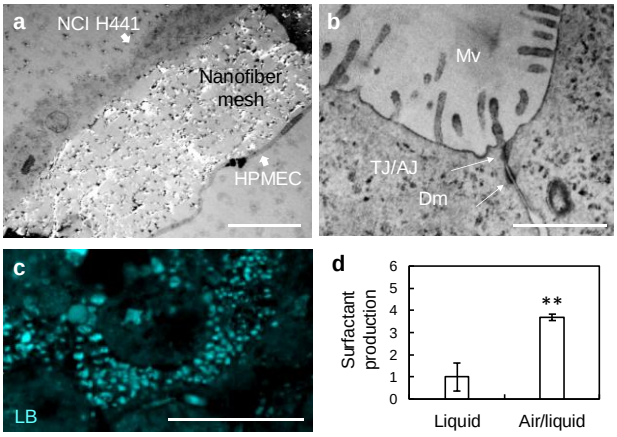

Figure 6. *Structural observation of bipolar cultured barriers. (a,b) TEM micrographs of bipolar cultured model of NCI H441 and HPMEC on nanofiber mesh after 7 days of incubation (Mv: microvilli, TJ/AJ: tight junction and adherens junction, Dm: desmosome). Mv at the apical membrane and TJ accompanied by AJ and Dm were confirmed. (c) Surfactant production of NCI H441 barriers formed on nanofiber mesh in liquid and air/liquid interface culture. LBs were stained with quinacrine. (d) Surfactant production of NCI H441 barriers formed on nanofiber mesh in liquid and air/liquid interface culture (n=3). LBs were stained with quinacrine. **P<0.01 when compared with liquid culture. Scale bars, 20 µm for (a), (c) and 1 µm for (b)*

3.7 Bipolar cultivation of primary alveolar-capillary model

In further experiments, we used primary human alveolar epithelial cells, i.e. type I and type II pneumocytes. Type I alveolar epithelial cells cover 95% of the alveolar barrier and conduct the gas exchange and transport of ions and fluids. Type II alveolar epithelial cell provide fluid homeostasis and immunological reaction by producing lung surfactant.[35] Human pulmonary alveolar epithelial cells (HPAEC) and primary human pulmonary microvascular endothelial cells (HPMEC) were used to reconstruct bipolar barriers. Since HPAEC may differentiate to type I phenotype during pre-culture on a plastic dish for the expansion and long term culture, only HPAEC with less than 2 passages were employed in order to control the ratio of type I and type II cells. The primary human HPAEC and HPMEC were separately cultivated on the opposite sides of the nanofiber mesh as described above and each cell type formed a confluent layer with adherens junction. This is demonstrated by the 3D-reconstructed confocal microscopy images of the bipolar barrier in **Figure 7a**. In contrast, our attempts with a conventional membrane with 3 µm pores demonstrated penetration of HPAEC through the pores and formation of rather imperfect heterocellular sheets at the endothelial side (**Figure 7b**). We compared the permeability between nanofiber mesh and porous films for an incubation for 6h by a dye transfer assay based on fluorescein isothiocyanate (FITC, hydrodynamic radius: <1 nm). We did not observe significant differences of the dye transfer between the plain nanofiber mesh and the porous membrane. However, when the cell barrier with NCI H441 was grown on the same substrates, the nanofiber mesh construct showed higher permeabil-

ity for FITC than the membrane construct (rate constant: 1.02 h^{-1} and 0.612 h^{-1}, respectively) (**Figure 7c**). The difference may be explained by the observation that the pores of the membrane became blocked by the infiltration of epithelial cells in conjunction with the fact that the porosity of the membrane was significantly lower than that of the nanofiber mesh (14% versus 71%). Obviously the rather open network hole structure of the nanofiber mesh allows a sufficiently direct contact and signal transfer between epithelial and endothelial cells and does not cause them to penetrate the networks. These results indicate a superior performance of the nanofiber mesh for bipolar cultivation.

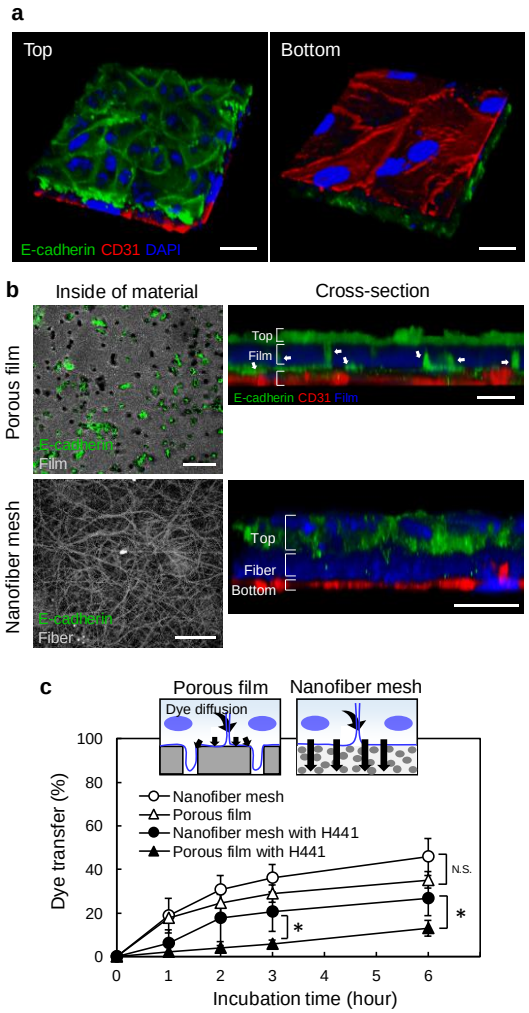

Figure 7. *Bipolar cultivation of primary alveolar-capillary cells. (a) 3D-reconstructed CLSM images of bipolar cultured HPAEC and HPMEC barriers. HPAEC and HPMEC were immune-stained with an anti-E-cadherin antibody (green) and an anti-CD31 antibody (red), respectively. The nuclei were stained with DAPI. (b) Comparison of primary barrier structures at the plane of membrane between porous film and nanofiber mesh. Cross-sectional CLSM image of the barrier prepared using porous film showed penetration of HPAEC through the pores and mixed layers on the bottom. (c) Dye transfer of FITC across porous film and nanofiber mesh without and with NCI H441 barriers (n=3). *P<0.05 when compared with porous film with NCI H441, N.S. denotes no significant difference. Scale bars, 20 µm.*

3.8 Triple-cultures seeded on basement membrane mimics: incorporation of THP-1

Prior to triple-culture experimentation, the acute human monocytic leukemia cell line THP-1 was seeded on fibronectin-coated 6-well-plates and treated with 8nM PMA for 4 days to induce macrophage differentiation into the pro-inflammatotry phenotype (M1). Characterization of macrophage-like phenotype was determined via immunofluorescent staining for macrophage specific marker CD105 and CD68. After 4 days of PMA treatment, adherent THP-1 cells revealed a typical macrophage-like morphology and stained positively for CD105 as well as CD68.

In the working group of Prof. Kirkpatrick, bipolar cell cultures consisting of NCI H441 and ISO-HAS-1 was performed on basement membrane mimics followed by addition of PMA treated THP-1 on the upper chamber of the transwells on top of the epithelial cells after 7 days of pre-cultured bipolar co-culture (**Scheme 2**).

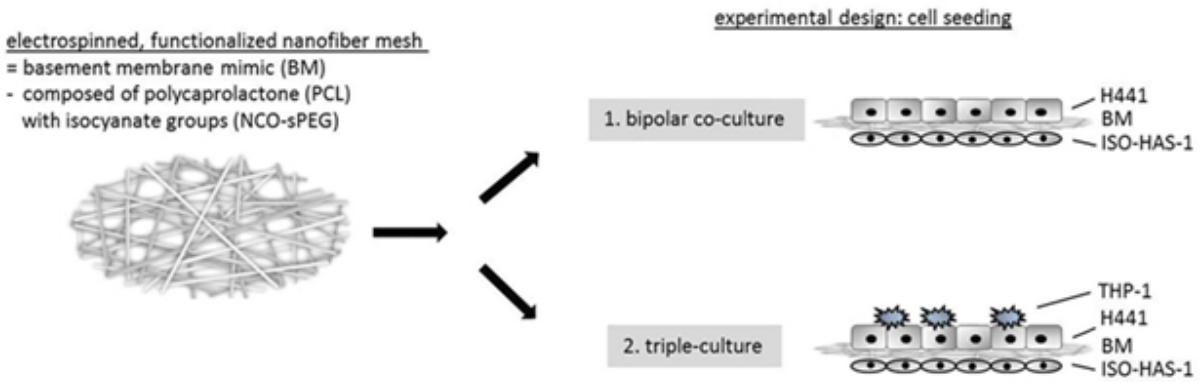

***Scheme 2**: schematic overview of the experimental setting. Bipolar co-culture consisting of NCI H441 and ISO-HAS-1 as well as triple-culture consisting of NCI H441, ISO-HAS-1 and THP-1 was seeded on an electrospinned, functionalized nanofiber mesh as a basement membrane mimic.*

Before starting the triple culture, TER needed to be measured (Ωcm^2 >300) for the bipolar culture as an essential prerequisite for seeding THP-1 to the bipolar culture. TER increased during the course of co-cultivation from 2 days to 7 days, reaching ~377 Ωcm^2 after 7 days of bipolar culturing. In response to macrophage treatment on day 7 (**Figure 8b, arrow**), TER decreased slightly over the period of triple cultivation up to 10 days (~329 Ωcm^2, figure 5b). In general, NCI H441 cells of alveolar barrier mimics composed of triple-culture, are organized in a more multi-layered structure (**Figure 8c**) compared to the barrier composed of the co-culture without THP-1, in which the epithelial cells formed a monolayer (**Fgure 7 a/b**). Immunohistochemical staining of the alveolar barrier mimics composed of NCI H441, ISO-HAS-1 and THP-1 for the macrophage marker CD105, revealed the distribution of the differentiated THP-1 cells in the *in vitro* system (**Figure 8c**). Detached CD105-positive cells, demonstrating the macrophage-like THP-1, are incorporated into the NCI H441 cell layer within the alveolar barrier mimic in the triple-culture (**Figure 8c, arrows**). The addition of macrophages to the established bipolar culture is mandatory in the study of possible lung inflammatory reactions *in vitro*, as it represents a more complex and relevant system by combining endothelial, epithelial and immune cells [36, 37]. Triple-cultures of THP-1 macrophages, NCI H441 epithelial cells and ISO-HAS-1 endothelial cells on the basement membrane mimic leads to a thicker membrane when compared to the bipolar co-culture, since the epithelial cells seem to organize into a multilayer when macrophages were added to the system. Macrophages can be found on top of the epithelial cell layer as well as on the bottom, adjacent to the basement membrane mimic, thus indicating a migrating property of the THP-1 in this system. TER decreased slightly after macrophage treatment of the co-culture but still remained at a high level, demonstrating an intact barrier even in response to macrophage treatment. In order to defend the host against exogenous pathogens, macrophages and alveolar epithelial cells represent the first line of defence [38]. Upon pathogen recognition, a definitive and orchestrated program of defence is activated and involves macrophage-mediated

inflammatory cytokine production, which finally triggers the response to the pathogen by activating the epithelial cells [39]. A number of studies focus on the pathogen or nanoparticle-defending role of macrophages in different settings of *in vitro* alveolar barrier models [36, 37, 40]. However, we have not yet been able to use the described model for the study of possible pathogenic or toxic effects of nanoparticles on the *in vitro* alveolar barrier system. The purpose of the present experimental work was to establish whether the rather non-physiological polycarbonate membrane of the Transwell® system could be replaced by a thinner, nanostructured bioresorbable membrane, and serve as a suitable substratum for double and triple co-cultures of the alveolar-capillary barrier. The data clearly demonstrate that suitable cell lines of human epithelial, endothelial and immune cells can indeed establish and maintain the barrier properties of the air-blood barrier on this novel membrane. It is hoped that this system will serve as a highly beneficial tool to test different pathogenic stimuli and thus provide a basis for better understanding of the physiology and pathology of the lung.

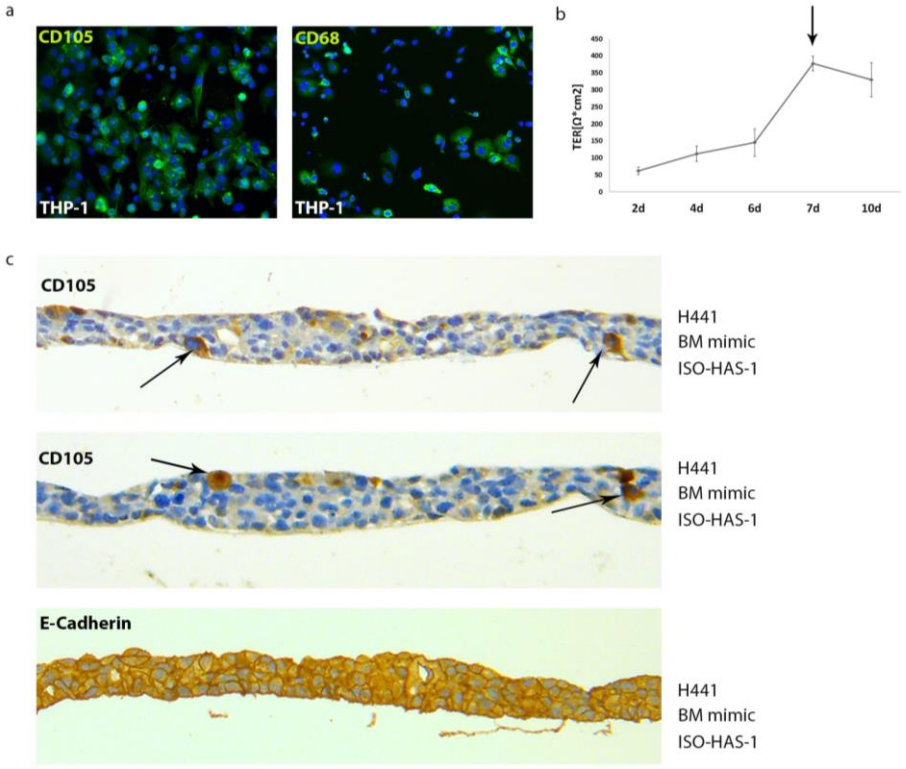

***Figure 8**: Triple culture experimentation. a/b. Characterization of PMA treated THP-1 cells via immunofluorescent staining for macrophage-marker CD105 (a) and CD68 (b). c. Barrier properties of in vitro triple culture model seeded on basement membrane mimics (=TER [Ω*cm^2]). c. Immunostaining of histological section of triple-cultured basement membranes for macrophage-marker CD105 and adherens junction protein E-Cadherin. Scale bars: a=75µm; c=50µm.*

3.9 Biodegradability test and ECM deposition

Finally, we tested the biodegradability of the nanofiber meshes under physiological conditions. The degradability of each mesh was evaluated from the weight loss it suffered during one month incubation at 37°C in culture media. PCL is expected to be hydrolyzed. However, in spite of the small diameter of the fibrils and the corresponding high surface to volume ratio, the degradation rate was extremely slow (1% in weight for 1 month). In order to accelerate the degradability, we employed micro/nanofiber mesh of poly(lactic-co-glycolic acid) (PLGA, 50/50). Under the same conditions, PLGA meshes showed more than 20 times higher weight

loss than PCL meshes. This is expected to favor the substitution of the artificial scaffold by natural ECM proteins. Collagen deposition secreted from cells was confirmed by a hydroxyproline assay although the amount of deposited collagen was small compared to that of the whole mesh. This ECM deposition is important not only to maintain the mechanical integrity as a basement membrane but should also improve self-regulation of cellular functions. A certain disadvantage of the PLGA fibers resulted from the inferior mechanical properties compared to PCL meshes, i.e. a larger hysteresis upon strain recovery. This problem can be overcome by the use of a mixture or copolymer of PCL and PLGA polymers that combine degradability and appropriate mechanical properties for mimicry of the basement membrane in an *in vitro* lung model.

Figure 9. *Degradation and ECM deposition. Degradability test of micro and nanofibers of PCL-sPEG and PLGA-sPEG (n=3) and collagen deposition in barriers with PLGA-sPEG nanofiber mesh. *P<0.05 when compared with PLGA microfiber. **P<0.01 when compared with day 7.*

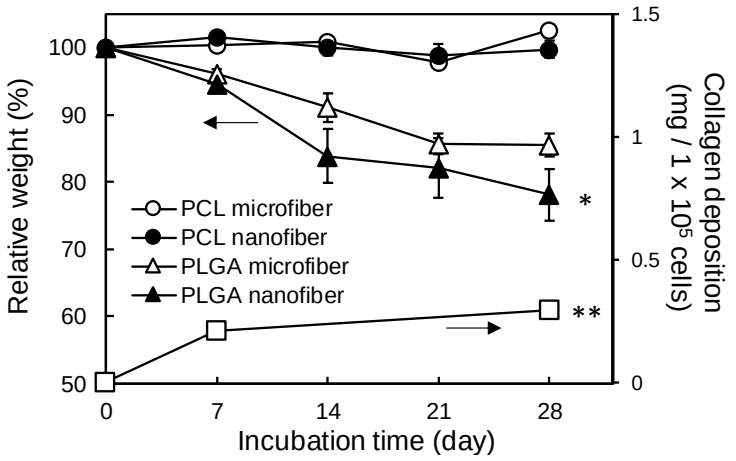

3.10 Design of a microfluidic cell culturing and oxygenator device

As step towards the *ex vivo* cultivation of a bipolar organ like alveolar barrier the group of Prof.Dr.-Ing. Matthias Wessling set up a multifunctional microfluidic device illustrated in Figure 1. The microfluidic device was designed with Autodesk Inventor 2017 and fabricated using polyjet 3D printing (Stratasys, Objet Eden 260V). The cell-culturing device was printed in a layer by layer fashion made of different materials. It consists of two flow chambers, one for the blood side and one for the bipolar alveolar barrier.

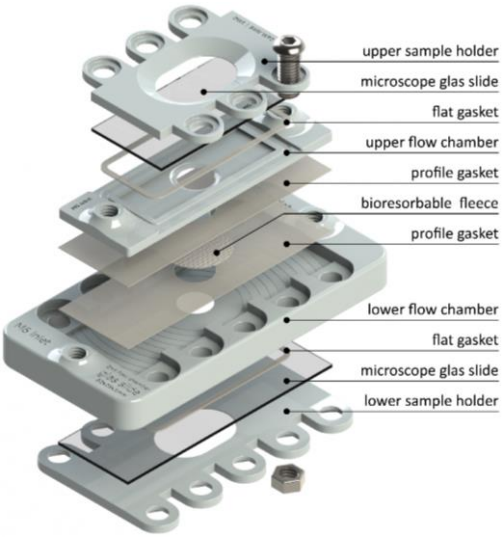

Figure 10: *Additive manufacture microfluidic cell culturing and oxygenator device*

The bioresorbable fleece can be fixed in between the two flow chambers and is sealed using custom-made PDMS profile gaskets. The two flow channels are sealed against microscope glass slides, which enable the observation of cell growth under an optical microscope during continuous flow cell-culturing experiments.

3.12 Cyto- and hemocompatibility evaluation and modification of the oxygenator device

The 3D printing materials were tested by IPF Dresden for cytotoxicity and the material properties were optimized towards an increased hemocompatibility. Cells are not intended to contact the device surface, but they can be exposed to leachable from the 3D printing polymer. Over-night extracts of hard and elastomeric 3D print polymers in cell culture medium were exposed to HUVEC cells on fibronectin coated tissue culture polystyrene. After 3 days the metabolic activity of the cells was determined by a PrestoBlue assay. The cured hard polymers VeroClear and RGD525 did not leach toxic substances, whereas extracts of the elastomers Tango+ and FLX950 suppressed the cell growth (**Figure 11**). PDMS therefore was used as elastomer for the gaskets.

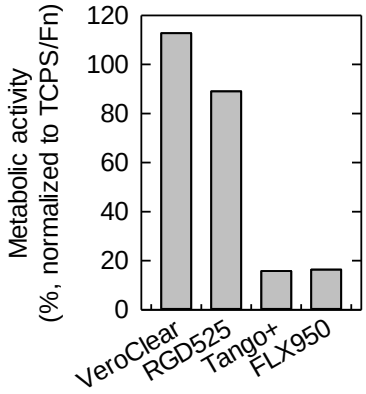

Figure 11: *Metabolic activity of HUVEC cells after three days exposure to extracts of 3D printing polymers.*

As the final device will be perfused with blood on one side, the blood compatibility of the polymers was probed by 2 hours incubation in 1 U/ml heparin anticoagulated whole blood against a Teflon® AF reference surface.[41] All 3D printing materials induced substantially higher coagulation activation (measured as prothrombin F1+2 fragment) and inflammatory complement activation (measured as complement fragment C5a) than the reference material (**Figure 12**), indicating low hemocompatibility of the polymers. Cellular parameters for blood platelet and granulocyte activation confirmed these observations (not presented).

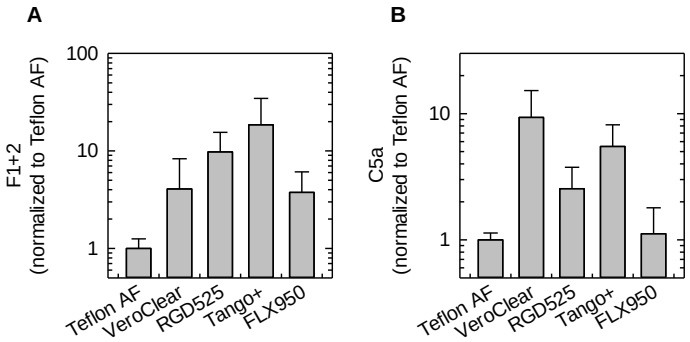

Figure 12: *Hemocompatibility of 3D printing polymers. A: Prothrombin F1+2 fragment as marker of coagulation activation. B: C5a as marker of inflammatory complement activation. Both parameters are normalized to the reference material Teflon AF as 1.*

As the bare surfaces of the 3D print polymers were not suitable for direct blood contact, they were coated with feedback controlled anticoagulant hydrogels (thrombin cleavable PEG-Heparin Gel, tcPHG). They consist of the anticoagulant heparin covalently linked with 4-armed PEG molecule (starPEG) *via* thrombin-cleavable linker peptides.[42, 43] Stable immobilization of the hydrogel requires amino- or carboxylic acid groups on the substrate. Low pressure air plasma treatment was shown to enhance the oxygen to carbon (O/C) ratio in the surface of RGD525 from 25% to 45%, suggesting also the formation of reactive carboxylic acid groups. Both the plasma- and untreated surface of RGD525 were capable to bind stably the hydrogel for more than 3 weeks in PBS. The hydrogel coating suppressed the coagulation and inflammation activation of the surfaces (**Figure 13** A, B).

As plasma treatment cannot activate inner and covered surfaces of the flow chamber, in a proof-of-principle study, thin films of non-cleavable hydrogel were polymerized directly on the blood connecting path of the chamber. The coated chamber was perfused with 1.5 U/ml heparinized blood for 2 hours in an oscillating mode with 4 ml/min; an uncoated chamber and a pure PVC tubing served as controls. Substantially reduced coagulation activation was observed with the coated chamber compared to the controls (**Figure 13** C). Non-specific heparin-release however still has to be excluded in this case.

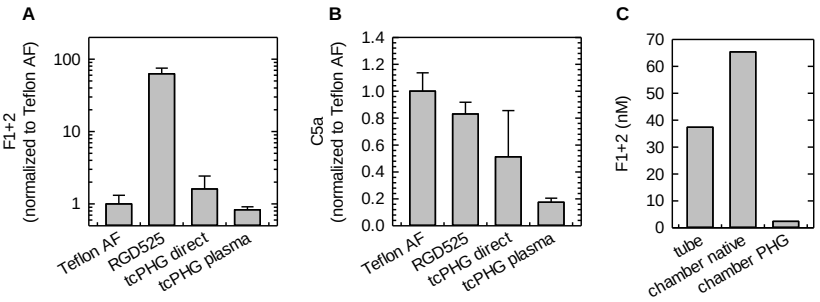

Figure 13: *Hemocompatibility of thrombin-cleavable PEG-Heparin Gel (tcPHG) coating on PHG525 without and with air plasma activation of the surface. A: Prothrombin F1+2 fragment as marker of coagulation; B: C5a as marker of complement activation. Both parameters normalized to Teflon AF as 1. C: Coagulation activation of a PEG-heparin gel (PHG) coated perfusion chamber compared to the*

uncoated chamber and a bare PVC tube.

3.13 Fabrication and operation of a microfluidic cell culturing and oxygenator device

The final device was made of the material MED610 (Stratasys) or RGD 525. The printed devices were post cured at 60°C under UV light exposure for 12 hours and sterilized using ethanol. In order to operate the device under physiological cell-culturing conditions the inner design of the cell-culturing device especially the round shaped diameter of the bioresorbable fleece/membrane was adapted to implement growth under a fluctuating tidal strain of the alveolar blood-air barrier of maximal 4 % at 8 mbar trans-membrane/-pulmonary pressure.[44, 45] The tidal strain was implemented using a setup including a reservoir, a peristaltic pump and two pressure sensors measuring the fluctuating transmembrane pressure (TMP). This setup shown in **Figure 14a** was used to analyze the linear and fluctuating signal caused by the peristaltic pump (**Figure 14b**).

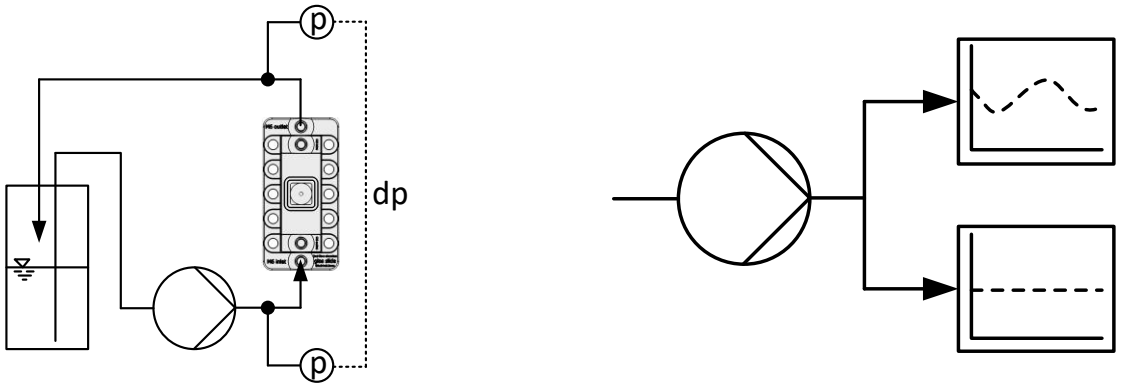

Figure 14a. *Continuous cell culturing setup including a reservoir, a peristaltic pump, two sensors and the microfluidic device with adapted membrane geometry.*

b. *Linear and fluctuating pressure signal caused by the peristaltic pump.*

The necessary TMP causing maximal 4 % tidal strain was evaluated using existing stress strain data measured by Akihiro et al. and simulated using the finite element method (FEM) as visualized in Figure 3a and b. Therefore the fleece was assumed to be a homogenous material with isotropic material properties (young's modulus: 25.1 MPa, shear modulus: 9.7 MPa, yield strength 1.4 MPa and tensile strength: 3.0 MPa) made with two different thickness of 55 µm and 13 µm. The FEM simulation allowed to change the design of the microfluidic device and were in the following used to calibrate the continuous cultivation process.

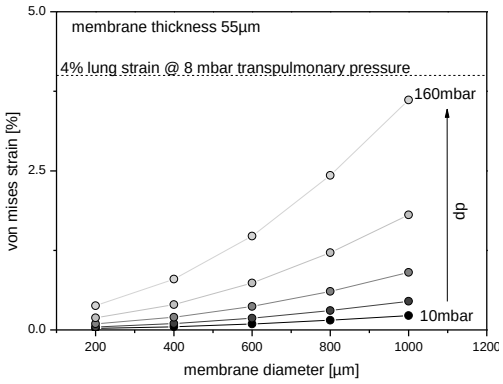

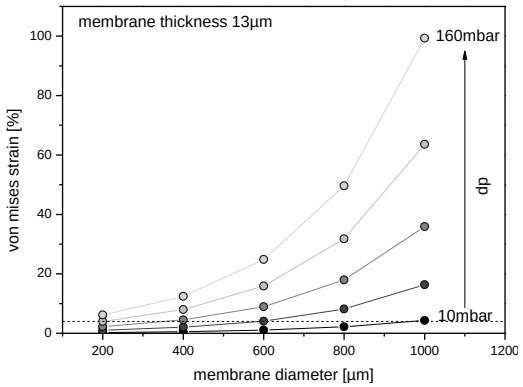

Figure 15a. *Strain behavior of a 55 µm thick membrane depended on the membrane diameter (0.2 - 1.0 mm) as well as the applied transmembrane pressure (10 – 160 mbar).*

b. *Strain behavior of a 13 µm thick membrane depended on the membrane diameter (0.2 – 1.0 mm) as well as the applied transmembrane pressure (10 – 160 mbar).*

For a membrane thickness of 55 µm the FEM simulations (**Figure 15a**) showed that a pressure of more than 160 mbar is necessary to achieve sufficient membrane strain. In comparison the 13 µm thick membrane (**Figure 15b**) has mechanical properties comparable the lung basement membrane and can be operated at vital conditions of around 10 mbar tidal pressure using a membrane diameter of 1.0 mm. For these conditions, the maximum strain was also analyzed to prevent irreversible plastic deformation damaging to the membrane. Apart from the simulation results, the microfluidic device was fabricated with a larger membrane diameter to increase the area for cell cultivation leading to a maximal TMP of 2.5 mbar to achieve 4% membrane strain (**Figure 16a**).

As shown in Figure 11b the setup was experimentally analyzed towards the applied linear and fluctuating pressure signal using the results of the FEM simulation. Physiological operation conditions were achieved at a Reynolds number of 3.5 (linear interpolation), that in this case equaled a flow rate of 1.5 ml min^{-1} (**Figure 16a**). The frequency of fluctuations caused by the peristaltic pump also fall in the range of the respiratory rates of children, adults and elderly people at rest (**Figure 16b**).

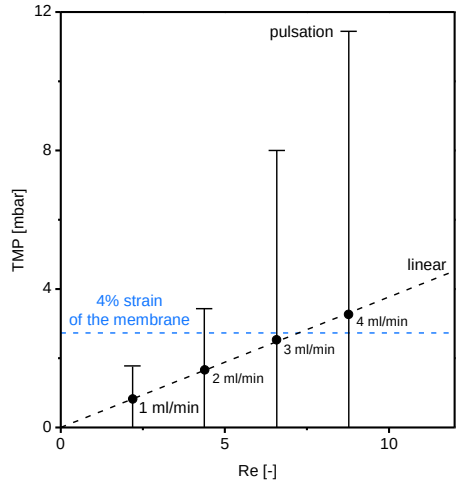

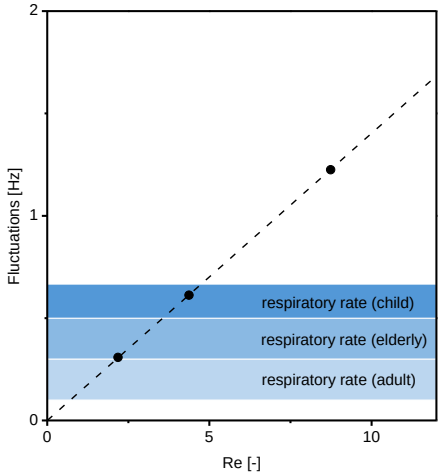

Figure 16a. *Linear and fluctuating pressure response of the peristaltic pump depended on the*

b. *Frequency of the applied fluctuating transmembrane pressure as a function of Reynolds*

flow rate, causing tidal strain of the membrane.

number. The frequency is compared to the respiratory rate of children, adults and elderly people.

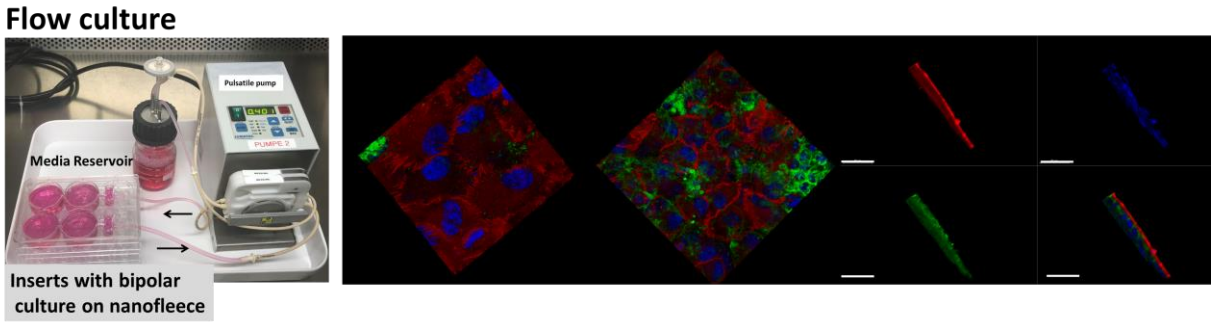

***Figure 17**: On left the flow setup is shown and on right is the confocal laser microscopy of the bipolar culture of NCI H441 and HUVEC on a further reduced nanofiber mesh of ~1.5µm thickness at a flow rate of 0.1dyne/cm^2. H441 and HUVEC are stained with immune-stained with an anti-E-cadherin antibody (green) and an anti-CD31 antibody (red), respectively. The nuclei were stained with DAPI. Scale is 50µm.*

4. Conclusion

In summary we developed bipolar cultured human primary alveolar-capillary barrier models using fully-synthetic nanofiber basement membrane mimics. One-step electrospinning process provided bioresorbable ultrathin nanofiber mesh with interconnected pores capable of cell-cell crosstalk. The nanofiber surface hydrophilized and decorated with sPEG and bioactive ligands suppressed unspecific protein adsorption and enhanced ligand-specific cellular adhesion. Biofunctionalized nanofiber mesh allowed for bipolar cultivation of confluent human primary epithelial and endothelial cell layers with fundamental alveolar functionality. Nanofiber mesh revealed higher mass transport as compared to conventional porous film due to high porosity and separate culture of cell layers. The use of PLGA improved the rate of biodegradability of nanofiber mesh and showed the replacement to natural ECMs, which highlighted the adjustability of synthetic materials. To test different pathogenic stimuli and thus provide a basis for better understanding of the physiology and pathology of the lung triple co-cultures of the alveolar-capillary barrier was established. For triple-cultures THP-1 macrophages were seeded on the alveolar barrier of epithelial cells and endothelial cells on the basement membrane mimic. This lead to multilayer of epithelia layer compared to the bipolar co-culture. Macrophages were found on top of the epithelial cell layer as well as on the bottom, adjacent to the basement membrane mimic, thus indicating a migrating property of the THP-1 in this system. TER decreased slightly after macrophage treatment of the co-culture but still remained at a high level, demonstrating an intact barrier even in response to macrophage treatment. The design and fabrication of a microfluidic cell-culturing device was successfully implemented. The continuous cell culturing process was optimized towards physiological conditions mimicking the alveolar environment where the cells can be cultivated

under a tidal strain. However as plasma treatment cannot activate inner and covered surfaces of the flow chamber, in a proof-of-principle study, thin films of non-cleavable PEG hydrogel were polymerized directly on the blood connecting path of the chamber which considerably reduced coagulation. But scientific challenge still lies in making the coating robust and stimuli sensitive, for long term heparin release which limited the establishment of the air-blood interface.

Conceivable follow-up projects

The results of our project clearly demonstrate that this system will serve as a highly beneficial tool for better understanding of molecular mechanisms in physiology and pathology of the lung. On this basis, we would like to extend our model and incorporate patient-specific primary cells to develop personalized lung models of health and disease. The model will be used to study the interactions of the lung with stimuli such as drugs, environmental agents, and consumer products etc. Since basement membrane exists in various barriers such as skin (epidermal-dermal barrier) and glomeruli in the kidney (blood-urine barrier), further projects, using the developed artificial basement membrane for *in vitro* tissue reconstruction will be conceived.

Publications from the project

1. Basement Membrane Mimics of Biofunctionalized Nanofibers for a Bipolar-Cultured Human Primary Alveolar-Capillary Barrier Model: Nishiguchi A, Singh S, Wessling M, Kirkpatrick CJ, Möller M, **Biomacomolecules.** 2017, 18(3): 719-727.
2. Human co- and triple-culture model of the alveolar-capillary barrier on a basement membrane mimic: Dohle E, Singh S, Nishiguchi A, Fischer T, Wessling M, Möller M, Sader R, Kasper JY, Ghanaati S, Kirkpatrick CJ, **Tissue Eng Part C Methods.** 2018, doi: 10.1089/ten.TEC.2018.0087
3. Microfluidic cell mimicking physiological conditions of the alveolar environment for establishment of alveolar-capillary barrier: Loelsberg J, Möller M., Wessling M (**to be submitted**)
4. Ultra-thin biofunctionalised alveolar-capillary basement membrane mimics : Getting closer to nature: Jain P, Singh S, Möller M (**to be submitted**)

References

1. B. Maher, *Nature*, 2013, **499**, 20-22.
2. A. M. Kloxin, C. J. Kloxin, C. N. Bowman and K. S. Anseth, *Adv Mater*, 2010, **22**, 3484-3494.
3. H. Yoshida, M. Matsusaki and M. Akashi, *Advanced Functional Materials*, 2009, **19**.
4. G. P. Raeber, M. P. Lutolf and J. A. Hubbell, *Biophysical journal*, 2005, **89**, 1374-1388.
5. Y. Haraguchi, T. Shimizu, M. Yamato and T. Okano, *RSC Advances*, 2012, **2**, 2184-2190.
6. Z. J. Gartner and C. R. Bertozzi, *Proceedings of the National Academy of Sciences*, 2009, **106**, 4606-4610.
7. A. Nishiguchi, H. Yoshida, M. Matsusaki and M. Akashi, *Adv Mater*, 2011, **23**, 3506-3510.
8. E. S. Place, N. D. Evans and M. M. Stevens, *Nature materials*, 2009, **8**, 457-470.
9. P. Gehr, M. Bachofen and E. R. Weibel, *Respiration Physiology*, 1978, **32**, 121-140.
10. J. P. Wikswo, *Experimental biology and medicine (Maywood, N.J.)*, 2014, **239**, 1061-1072.
11. M. I. Hermanns, R. E. Unger, K. Kehe, K. Peters and C. J. Kirkpatrick, *Laboratory investigation; a journal of technical methods and pathology*, 2004, **84**, 736-752.
12. M. I. Hermanns, S. Fuchs, M. Bock, K. Wenzel, E. Mayer, K. Kehe, F. Bittinger and C. J. Kirkpatrick, *Cell and tissue research*, 2009, **336**, 91-105.

13. K. L. Sellgren, E. J. Butala, B. P. Gilmour, S. H. Randell and S. Grego, *Lab Chip*, 2014, **14**, 3349-3358.
14. D. Huh, B. D. Matthews, A. Mammoto, M. Montoya-Zavala, H. Y. Hsin and D. E. Ingber, *Science*, 2010, **328**, 1662-1668.
15. A. O. Stucki, J. D. Stucki, S. R. Hall, M. Felder, Y. Mermoud, R. A. Schmid, T. Geiser and O. T. Guenat, *Lab Chip*, 2015, **15**, 1302-1310.
16. L. G. Dobbs, *The American journal of physiology*, 1990, **258**, L134-147.
17. D. Huh, H. Fujioka, Y.-C. Tung, N. Futai, R. Paine, J. B. Grotberg and S. Takayama, *Proceedings of the National Academy of Sciences*, 2007, **104**, 18886-18891.
18. R. Kalluri, *Nature reviews. Cancer*, 2003, **3**, 422-433.
19. G. Zimmerman and H. Soreq, *Cell and tissue research*, 2006, **326**, 655-669.
20. Y. Yamada, K. Hozumi and M. Nomizu, *Chemistry – A European Journal*, 2011, **17**, 10500-10508.
21. I. Garip) Yasa, N. Gunduz, M. Kilinc, M. Guler and A. Tekinay, *Basal Lamina Mimetic Nanofibrous Peptide Networks for Skeletal Myogenesis*, 2015.
22. D. Grafahrend, K.-H. Heffels, M. V. Beer, P. Gasteier, M. Möller, G. Boehm, P. D. Dalton and J. Groll, *Nat. Mat.*, 2011, **10**, 67–73.
23. B. M. Baker, B. Trappmann, W. Y. Wang, M. S. Sakar, I. L. Kim, V. B. Shenoy, J. A. Burdick and C. S. Chen, *Nature materials*, 2015, **14**, 1262-1268.
24. I. Keun Kwon, S. Kidoaki and T. Matsuda, *Biomaterials*, 2005, **26**, 3929-3939.
25. S. Y. Chew, R. Mi, A. Hoke and K. W. Leong, *Advanced Functional Materials*, 2007, **17**, 1288-1296.
26. H. Gotz, U. Beginn, C. F. Bartelink, H. J. M. Grunbauer and M. Moller, *Macromol Mater Eng*, 2002, **287**, 223-230.
27. K. Klinkhammer, J. Bockelmann, C. Simitzis, G. A. Brook, D. Grafahrend, J. Groll, M. Möller, J. Mey and D. Klee, *J. Mater. Sci. Mater. Med.*, 2010, **21**, 2637–2651.
28. J. Groll, Z. Ademovic, T. Ameringer, D. Klee and M. Moeller, *Biomacromolecules*, 2005, **6**, 956-962.
29. J. Groll, T. Ameringer, J. P. Spatz and M. Moeller, *Langmuir : the ACS journal of surfaces and colloids*, 2005, **21**, 1991-1999.
30. L. D. Shea, D. Wang, R. T. Franceschi and D. J. Mooney, *Tissue Engineering*, 2000, **6**, 605-617.
31. K. G. Birukov, J. R. Jacobson, A. A. Flores, S. Q. Ye, A. A. Birukova, A. D. Verin and J. G. N. Garcia, *American Journal of Physiology-Lung Cellular and Molecular Physiology*, 2003, **285**, L785-L797.
32. B. D. Ratner and S. J. Bryant, *Annual review of biomedical engineering*, 2004, **6**, 41-75.
33. S. Ali, J. E. Saik, D. J. Gould, M. E. Dickinson and J. L. West, *BioResearch open access*, 2013, **2**, 241-249.
34. J. Salber, S. Gräter, M. Harwardt, M. Hofmann, D. Klee, J. Dujic, H. Jinghuan, J. Ding, S. Kippenberger, A. Bernd, J. Groll, J. P. Spatz and M. Möller, *Small*, 2007, **3**, 1023-1031.
35. M. A. Matthay, H. G. Folkesson and C. Clerici, *Physiological reviews*, 2002, **82**, 569-600.
36. J. Y. Kasper, M. I. Hermanns, R. E. Unger and C. J. Kirkpatrick, *J Tissue Eng Regen Med*, 2017, **11**, 1285-1297.
37. S. G. Klein, T. Serchi, L. Hoffmann, B. Blomeke and A. C. Gutleb, *Particle and fibre toxicology*, 2013, **10**, 31.
38. L. A. Pittet, L. J. Quinton, K. Yamamoto, B. E. Robson, J. D. Ferrari, H. Algul, R. M. Schmid and J. P. Mizgerd, *American journal of respiratory cell and molecular biology*, 2011, **45**, 573-581.
39. M. R. Jones, B. T. Simms, M. M. Lupa, M. S. Kogan and J. P. Mizgerd, *J Immunol*, 2005, **175**, 7530-7535.
40. C. Schulz, X. Lai, W. Bertrams, A. L. Jung, A. Sittka-Stark, C. E. Herkt, H. Janga, K. Zscheppang, C. Stielow, L. Schulte, S. Hippenstiel, J. Vera and B. Schmeck, *Scientific reports*, 2017, **7**, 11988.
41. U. Streller, C. Sperling, J. Hubner, R. Hanke and C. Werner, *Journal of biomedical materials research. Part B, Applied biomaterials*, 2003, **66**, 379-390.
42. M. F. Maitz, U. Freudenberg, M. V. Tsurkan, M. Fischer, T. Beyrich and C. Werner, *Nature communications*, 2013, **4**, 2168.
43. M. F. Maitz, J. Zitzmann, J. Hanke, C. Renneberg, M. V. Tsurkan, C. Sperling, U. Freudenberg and C. Werner, *Biomaterials*, 2017, **135**, 53-61.
44. E. Roan and C. M. Waters, *Am J Physiol Lung Cell Mol Physiol*, 2011, **301**, L625-635.
45. R. M. S. Kacmarek, J. K.; Heuer A., 2017.